JOURNAL OF MAGNETIC RESONANCE **133,** 21–35 (1998)
ARTICLE NO. MN981423

Temporal Characteristics of NMR Signals from Spin 3/2 Nuclei of Incompletely Disordered Systems

Donald E. Woessner[1] and Navin Bansal

The University of Texas Southwestern Medical Center at Dallas, Department of Radiology, Rogers Magnetic Resonance Center, 5801 Forest Park Road, Dallas, Texas 75235-9085

Received September 8, 1997

Anisotropic nuclear quadrupole interactions can produce residual quadrupole splitting in the NMR spectra of rapidly moving quadrupolar nuclei in incompletely disordered aqueous heterogeneous systems. Such systems may include hydrated sodium nuclei in biological tissue and biopolymer gels. To describe the NMR signals from such samples, we use a domain model in which each domain is characterized by a quadrupole frequency and a residence time of the nucleus. We show that the signals from each domain after one pulse, the quadrupole echo sequence, and the various multiple quantum filters (MQFs) can be expressed as a linear combination of five different phase coherences. To simulate the effect of various distributions (Pake powder pattern, Gaussian, etc.) of quadrupole frequencies for different domains on the NMR signal, we have written the computer program CORVUS. CORVUS also includes the effects of exchange between different domains using diffusion and random jump models. The results of computer simulations show that the Gaussian and Pake powder pattern quadrupole frequency distributions produce very different phase coherences and observable NMR signals when the exchange rate ($1/\tau_e$) between different domains is slow. When $1/\tau_e$ is similar to the root mean square quadrupole frequency (σ), the signals from the two distributions are similar. When $1/\tau_e$ is an order of magnitude greater than σ, there is no apparent evidence of quadrupole splitting in the shape of the signal following one pulse, but the residual effects of the quadrupole splitting make a significant contribution to the fast transverse relaxation rate. Therefore, in this case, it is inappropriate to use the observed biexponential relaxation rates to obtain a single correlation time. The quadrupole echo and the various MQF signals contain an echo from the satellite transitions in the presence of quadrupole splitting. The peak of this echo is very sensitive to $1/\tau_e$. The time domain analysis of these signals is more direct and less ambiguous than the frequency domain analysis because the echo does not occur at the beginning of data acquisition. The quadrupole echo pulse sequence is the most sensitive detector of residual quadrupole splitting and exchange of sodium ions between different domains. However, if the sample is compartmentalized so that only a fraction of the nuclei have quadrupole splitting, the double quantum magic angle filter (DQ-MA) is more suitable. This is because the DQ-MA signal contains only the contributions from satellite transitions. Use of simulations to analyze signals from various one-pulse, quadrupole echo, and multiple quantum filter pulse sequences can yield information on substrate order and aid in quantitation of multiple quantum filter signals. © 1998 Academic Press

Key Words: **coherences; exchange; order; quadrupole splitting; transverse relaxation.**

INTRODUCTION

There is considerable interest in ^{23}Na quadrupole splitting in biological tissue such as cartilage, skeletal muscle, and brain (*1, 2*). It has long been known that, because of anisotropic interactions, NMR signals of quadrupolar nuclei such as ^{2}H in aqueous, locally ordered systems such as xanthan gum and montmorillonite clay exhibit nonzero residual quadrupole splitting (*3, 4*). This splitting depends on the local order of the macromolecules and clay sheets. For any given nucleus, molecular diffusion in the sample causes its quadrupole frequency to be time dependent. In like fashion, the ^{23}Na NMR signals from samples such as biological tissue and biopolymer solutions and gels are also expected to be affected by macromolecular order and time dependence of the quadrupole frequency. Hence, we should obtain information on the substrate structure and order from analysis of NMR signals following appropriate RF pulse sequences.

To obtain this structural information from spin 3/2 NMR data, we use simulations based on a general mathematical model. In this model the various NMR signals depend on the conventional relaxation rates and quadrupole frequencies and are expressed as linear combinations of phase coherences. This formulation can encompass various physical models of aqueous heterogeneous systems involving different distributions of quadrupole frequencies and time dependences of these frequencies.

For the simulation and analysis of spin 3/2 data from partially ordered systems, we use the domain model that was developed to analyze the NMR signals from ^{2}H nuclei of water in aqueous heterogeneous systems (*3, 5, 6*). In this model, the sample comprises domains that are nonrandom arrangements of macromolecules with which the fluid molecules and hydrated ions interact anisotropically. The local rotational and

[1] To whom correspondence should be addressed.

1090-7807/98 $25.00

translational motions of water molecules and hydrated ions in a domain are rapid and contribute to the spectral densities $J_0(0)$, $J_1(\omega_0)$, and $J_2(2\omega_0)$ that determine the conventional transverse relaxation rates s_1 and s_2. In other words, within a very short period of time, these rapid motions cause a given spin 3/2 nucleus to experience all of the different kinds of local environments (''bulk'' aqueous phase, specific binding sites on the macromolecules, and nonspecific binding sites on the macromolecules) within the domain; all nuclei in the domain have the same relaxation times. The local anisotropic interactions of ions with a given macromolecule, together with the nonrandom arrangement of macromolecules in the domain, cause the nucleus to experience a small residual electrostatic field gradient (efg). This efg is characterized by the principal value eq along its major axis, whose orientation is determined by the domain orientation, and the asymmetry parameter η. Thus, the domain is characterized by a value of quadrupole frequency ω_Q that depends on the orientation of the domain in $\mathbf{B}_0$. The fundamental cause of the local residual efg is the presence of the macromolecules. These macromolecules may have electric charges and local electric dipole moments and also cause distortion of the hydration atmosphere of the ions.

If all the domains have the same residual efg and are parallel, the sample is a liquid crystal that gives narrow lines in the NMR spectrum. If the molecules and hydrated ions are constrained within given domains and if the different domains are randomly oriented with respect to $\mathbf{B}_0$, the NMR spectrum is the Pake powder pattern. Samples that have domains of a wide range of eq and η values (poorly ordered) can have a distribution of ω_Q values that is approximately Gaussian. In all these cases, we define the quantity σ^2 as the average of the ω_Q^2 values taken over all the domains. Because translational diffusion causes molecules and ions to migrate between domains, the ω_Q values that the nuclei experience are time dependent. We describe this time dependence in terms of τ_e, the average time that a nucleus resides in a given domain. The domain size and the translational diffusion coefficient determine the value of τ_e. This is an exchange process with the consequent line broadening and line narrowing effects that modify the NMR signals from various pulse sequences (*7*).

To explain the biexponential transverse relaxation character of ^{23}Na NMR signals of biological tissue, Berendsen and Edzes proposed (*8*) a fast-exchange domain-type model in which $\sigma\tau_e \ll 1$. Later, the transverse relaxation of ^{23}Na in dilute polyelectrolyte solutions was explained (*9*) by a similar fast-exchange model. Springer (*10*) has recently concluded that a model of the Berendsen type is the most realistic one, among several possible alternatives, for the description of ^{23}Na signals in biological tissue.

Recent papers report ^{23}Na quadrupole splitting in xanthan gum solutions (*11*) and κ-carrageenan solutions (*12*) that depends on sample preparation. Also, ^{23}Na in articular cartilage shows quadrupole splitting that depends sample compression (*13*). These observations suggest that biopolymer gels and biological tissue (*1, 2*) may not always be in the limiting case of $\sigma\tau_e \ll 1$ and that it is appropriate to examine the general case. Simulations in terms of the structural parameters σ, η, and τ_e facilitate the analysis of observed signals. A preliminary report (*14*) on the analysis of ^{23}Na NMR signals from a 20% xanthan gum solution illustrates an application of this procedure.

In this paper we carry out an elementary density matrix calculation of the transverse magnetization for spin 3/2 nuclei that have a constant quadrupole interaction and apply this calculation to one-pulse and two-pulse sequences. The NMR signals from these RF pulse sequences are expressed as linear combinations of two and five phase coherences, respectively. Various multiple quantum filter signals are also expressed as linear combinations of the same five phase coherences. The NMR signals are calculated for several distributions of constant quadrupole frequencies. Then, the quadrupole frequency for a given nucleus is allowed to be time dependent due to various models of motion. The effects of such time dependences on various NMR signals are examined. Finally, we draw implications of these time dependences for the interpretation of NMR data from incompletely disordered systems.

EXPRESSION OF NMR SIGNALS AS SUMS OF PHASE COHERENCES

Density Matrix Calculation of Transverse Magnetization with Quadrupole Splitting

The density matrix method is used to calculate the NMR signals for spin 3/2 nuclei that experience a residual nuclear quadrupole interaction. Initially, we assume that this quadrupole interaction is constant. The effects of time dependence of the quadrupole interaction are considered after the basic functions that describe the transverse magnetization are derived. In this calculation (*15*), the total nuclear spin wave function Ψ is

$$\Psi = c_1\phi_{3/2} + c_2\phi_{1/2} + c_3\phi_{-1/2} + c_4\phi_{-3/2} = \sum_{n=1}^{4} c_n u_n, \quad [1]$$

where ϕ_m are the orthonormal spin functions for the four m values of the nucleus. We assume that the quadrupole interaction is much smaller than the Zeeman interaction and write the Hamiltonian $\mathcal{H}$ as the sum of these two interactions:

$$\mathcal{H} = \mathcal{H}_z + \mathcal{H}_Q. \quad [2]$$

For spin I = 3/2,

$$\mathcal{H}_z = -\gamma\hbar B_0 I_z \quad [3]$$

$$\mathcal{H}_Q = (e^2qQ/24)(3\cos^2\theta - 1 + \eta\sin^2\theta\cos 2\phi)(3I_z^2 - 15/4), \quad [4]$$

where γ is the nuclear magnetogyric ratio, $\hbar$ is Planck's constant divided by 2π, I_z is the nuclear spin angular momentum operator, eQ is the nuclear quadrupole moment, eq is the principal value of the residual efg along its major axis, θ and ϕ are the polar and azimuthal angles of the orientation of the efg major axis in $\mathbf{B}_0$, and η is the asymmetry parameter of the residual efg.

The energy levels are then

$$E_{3/2} = -(3/2)\gamma\hbar B_0 + (e^2qQ/8) \times (3\cos^2\theta - 1 + \eta\sin^2\theta\cos 2\phi) \quad [5]$$

$$E_{1/2} = -(1/2)\gamma\hbar B_0 - (e^2qQ/8) \times (3\cos^2\theta - 1 + \eta\sin^2\theta\cos 2\phi) \quad [6]$$

$$E_{-1/2} = (1/2)\gamma\hbar B_0 - (e^2qQ/8) \times (3\cos^2\theta - 1 + \eta\sin^2\theta\cos 2\phi) \quad [7]$$

$$E_{-3/2} = (3/2)\gamma\hbar B_0 + (e^2qQ/8) \times (3\cos^2\theta - 1 + \eta\sin^2\theta\cos 2\phi). \quad [8]$$

The observed pulse NMR free induction signals result from the average expectation value of the transverse nuclear spin magnetization, $\langle M_+\rangle$, that rotates about the direction of $\mathbf{B}_0$,

$$\langle M_+\rangle = \langle M_x + iM_y\rangle = \gamma\hbar\langle I_x + iI_y\rangle = \gamma\hbar\langle I_+\rangle, \quad [9]$$

where I_+ is the spin angular momentum raising operator. The density matrix method is used to calculate $\langle M_+\rangle$ as

$$\langle M_+\rangle = \mathrm{Tr}(\rho M_+), \quad [10]$$

where the matrix elements are

$$\rho_{nm} = c_n c_m^*, \quad [11]$$

$$M_{+nm} = \gamma\hbar(u_m|I_+|u_n). \quad [12]$$

From these equations, we find that

$$\langle M_+\rangle = \gamma\hbar(\sqrt{3}\rho_{21} + 2\rho_{32} + \sqrt{3}\rho_{43}). \quad [13]$$

The RF pulses establish initial conditions on the density matrix ρ by causing changes in the wavefunction Ψ:

$$\Psi \rightarrow P\Psi, \quad [14]$$

where the matrix P represents the action of the pulse and Ψ is written as a column matrix. The transformation matrix P is found by solving the Schroedinger equation. The details are not given here, since they are well known. To minimize the complexity of the results while retaining the essential features of the models described in this paper, we treat the on-resonance case with infinitely strong 90-degree pulses and perfectly homogeneous B_1 and $\mathbf{B}_0$. The effect of the pulse on the density matrix is represented by

$$\rho \rightarrow P\rho P^{-1}. \quad [15]$$

The spin system is at equilibrium before the application of the first RF pulse. The equilibrium density matrix ρ^0 has nonzero elements only along the diagonal. Because $\mathcal{H}_z \gg \mathcal{H}_Q$ in Eq. [2], and because the nuclear spin energy levels are small compared to kT, the diagonal elements of ρ^0 can be written as

$$\rho^0_{11} = 1/4 + 3\epsilon \quad [16]$$

$$\rho^0_{22} = 1/4 + \epsilon \quad [17]$$

$$\rho^0_{33} = 1/4 - \epsilon \quad [18]$$

$$\rho^0_{44} = 1/4 - 3\epsilon. \quad [19]$$

Then, because

$$M_0 = \gamma\hbar\ \mathrm{Tr}(\rho^0 I_z), \quad [20]$$

where I_z is the z-component of nuclear spin angular momentum, the value of ϵ is given by

$$\epsilon = M_0/(10\gamma\hbar), \quad [21]$$

where M_0 is the equilibrium longitudinal nuclear spin magnetization.

Between pulses, the interaction of the nuclear magnetic moment with the magnetic field $\mathbf{B}_0$ and the interaction of the nuclear quadrupole moment with the efg impose a time dependence on the density matrix as expressed by

$$d\rho/dt = (i/\hbar)[\rho, \mathcal{H}], \quad [22]$$

in which i is the imaginary quantity $\sqrt{-1}$ and $\mathcal{H}$ is given by Eqs. [2]–[4]. Application of this equation then yields the time dependence of the density matrix elements,

$$d\rho_{nm}/dt = (i/\hbar)[E_m - E_n]\rho_{nm}, \quad [23]$$

where E_m and E_n are the energy levels of the spin states m and n as given by Eqs. [5]–[8]. Then, with the definitions

$$\omega_0 = \gamma B_0 \quad [24]$$

$$\omega_Q = (\pi/2)\mathrm{QCC}(3\cos^2\theta - 1 + \eta\sin^2\theta\cos 2\phi), \quad [25]$$

where QCC is the residual quadrupole coupling constant (i.e., e^2qQ divided by Planck's constant), we use Eq. [23] to calculate the time dependence of the matrix elements. To include

relaxation, we introduce the transverse relaxation rates s_1 and s_2. These relaxation rates describe the effects of rapid local motions (faster than $1/\omega_Q$) that involve the electric dipole moments of water molecules and electric charges of macromolecules. The results are the following time dependences of the off-diagonal density matrix elements that are pertinent in one- and two-pulse experiments:

$$d\rho_{21}/dt = i(-\omega_0 + \omega_Q)\rho_{21} - s_1\rho_{21} \quad [26]$$

$$d\rho_{32}/dt = -i\omega_0\rho_{32} - s_2\rho_{32} \quad [27]$$

$$d\rho_{43}/dt = i(-\omega_0 - \omega_Q)\rho_{43} - s_1\rho_{43} \quad [28]$$

$$d\rho_{12}/dt = -i(-\omega_0 + \omega_Q)\rho_{12} - s_1\rho_{12} \quad [29]$$

$$d\rho_{23}/dt = i\omega_0\rho_{23} - s_2\rho_{23} \quad [30]$$

$$d\rho_{34}/dt = -i(-\omega_0 - \omega_Q)\rho_{34} - s_1\rho_{34}. \quad [31]$$

Phase Coherences for NMR Signal Following One 90° Pulse

We use conventional mathematical operations (4×4 matrix multiplications and elementary trigonometry) to evaluate the density matrix elements. By substituting these matrix elements into Eq. [13], we find that the transverse magnetization in uniform $\mathbf{B}_0$ following a 90° RF pulse applied in the *x*-direction generates the following in-phase on-resonance NMR signal in the ''real'' channel of the NMR receiver:

$$\begin{aligned} S(t) &= (2/5)\exp(-s_2t) + (3/5)\exp(-s_1t)\cos(\omega_Q t) \\ &= (2/5)\mathrm{PC1} + (3/5)\mathrm{PC2}. \end{aligned} \quad [32]$$

This signal is the sum of two phase coherences, PC1 and PC2. They are characterized at time *t* by an amplitude and an accumulated phase angle. The amplitude is determined by relaxation rates s_1 and s_2. The accumulated phase angle is the product $\omega_Q t$. Phase coherence PC1 arises from the ''central'' transition with frequencies that, to first order, are independent of the quadrupole interaction (i.e., from the density matrix element ρ_{32}). Phase coherence PC2 arises from the ''satellite'' transitions with frequencies that depend on the nuclear quadrupole interaction (i.e., from the density matrix elements ρ_{21} and ρ_{43}).

Phase Coherences for NMR Signals Following Two 90° Pulses and Multiple-Quantum Filters

The in-phase on-resonance quadrupole echo signal (QE) following two 90° RF pulses phase-shifted by 90° and the second pulse applied at the time τ after the first pulse is

$$\begin{aligned} \mathrm{QE}(t > \tau) = (2/20)\mathrm{PC1} - (3/20)\mathrm{PC2} + (6/20)\mathrm{PC3} \\ + (6/20)\mathrm{PC4} + (9/20)\mathrm{PC5}, \end{aligned} \quad [33]$$

where

$$\mathrm{PC1} = \exp[-s_2t] \quad [34]$$

$$\mathrm{PC2} = \exp[-s_1t]\cos[\omega_Q t] \quad [35]$$

$$\mathrm{PC3} = \exp[-s_1\tau]\exp[-s_2(t-\tau)]\cos[\omega_Q\tau] \quad [36]$$

$$\mathrm{PC4} = \exp[-s_2\tau]\exp[-s_1(t-\tau)]\cos[\omega_Q(t-\tau)] \quad [37]$$

$$\mathrm{PC5} = \exp[-s_1t]\cos[\omega_Q(t-2\tau)]. \quad [38]$$

If the second pulse has a 180° flip angle, the signal is the same as given by Eq. [32]. The reason is that the $+m$ and $-m$ spin energy levels have the same dependences on quadrupole splitting (see Eqs. [5]–[8]).

Several multiple quantum filters (MQF) consist of a pulse that is followed by a preparation time τ which is terminated by two pulses that are separated by an evolution time (*16*). When the evolution time is very short, the final two pulses comprise a composite pulse. Therefore, the transverse magnetization following the filter should contain the same coherences as the quadrupole echo signal, but with different numerical coefficients. The convention in this paper is that the first pulse defines time $t = 0$. The signal (*2*) following a double quantum filter (DQ) is then

$$\begin{aligned} \mathrm{DQ}(\tau, t-\tau) = -d^1_{10}(\theta)[d^2_{21}(\theta) + d^2_{2-1}(\theta)]^2 \\ \times q^{(1)}_{21}(t)q^{(1)}_{12}(t-\tau) \\ + d^1_{10}(\theta)[d^3_{21}(\theta) - d^3_{2-1}(\theta)]^2 \\ \times q^{(1)}_{31}(\tau)q^{(1)}_{13}(t-\tau) \end{aligned} \quad [39]$$

and the signal (*17*) following a triple quantum filter (TQ) is

$$\begin{aligned} \mathrm{TQ}(\tau, t-\tau) = d^1_{10}(\theta)[d^3_{31}(\theta) + d^3_{3-1}(\theta)]^2 \\ \times q^{(1)}_{31}(\tau)q^{(1)}_{13}(t-\tau), \end{aligned} \quad [40]$$

where the *d*'s are reduced rotation matrix elements (*18*) and the *q*'s are given (*2*) as

$$q_{21}(\tau) = i(3/5)^{1/2}\exp(-s_1\tau)\sin[\omega_Q\tau] \quad [41]$$

$$q_{12}(t-\tau) = i(3/5)^{1/2}\exp[-s_1(t-\tau)]\sin[\omega_Q(t-\tau)] \quad [42]$$

$$q_{31}(\tau) = (6/25)^{1/2}\{\exp[-s_1\tau]\cos[\omega_Q\tau] - \exp[-s_2\tau]\} \quad [43]$$

$$\begin{aligned} q_{13}(t-\tau) = (6/25)^{1/2}\{\exp[-s_1(t-\tau)] \\ \times \cos[\omega_Q(t-\tau)] - \exp[-s_2(t-\tau)]\}. \end{aligned} \quad [44]$$

By expanding Eqs. [39] and [40] and rearranging terms, we can express the NMR signals from the quadrupole echo sequence and the various multiple quantum filters in the form

$$\begin{aligned} S(t > \tau) = c1\ \mathrm{PC1} + c2\ \mathrm{PC2} + c3\ \mathrm{PC3} \\ + c4\ \mathrm{PC4} + c5\ \mathrm{PC5}. \end{aligned} \quad [45]$$

TABLE 1
Numerical Coefficients c_i of the Various Phase Coherences in NMR Signals from One-Pulse, Quadrupole Echo, and Several Multiple Quantum Filter Sequences

Phase coherence	One-pulse	QE	TQ	DQ	DQ-MA	Composite (3DQ − 2TQ)
PC1	2/5	1/10	$-(9/40)/\sqrt{2}$	$(6/40)/\sqrt{2}$	0	0
PC2	3/5	−3/20	$-(9/80)/\sqrt{2}$	$(3/8)/\sqrt{2}$	$(1/5)/\sqrt{2}$	$(9/50)/\sqrt{2}$
PC3	0	3/10	$(9/40)/\sqrt{2}$	$-(6/40)/\sqrt{2}$	0	0
PC4	0	3/10	$(9/40)/\sqrt{2}$	$-(6/40)/\sqrt{2}$	0	0
PC5	0	9/20	$-(9/80)/\sqrt{2}$	$-(9/40)/\sqrt{2}$	$-(1/5)/\sqrt{2}$	$-(9/50)/\sqrt{2}$

The numerical coefficients for the DQ and TQ signals and also those for the one-pulse and QE cases are given in Table 1. The magic angle filter (DQ-MA), which is the DQ filter that is modified by making the flip angles of the second and third pulses be magic angle pulses, is especially useful because phase coherences PC1, PC3, and PC4 are absent. To achieve this result, accuracy of flip angle is very important. The DQ and TQ filters are less sensitive to accuracy of flip angle. A composite filter made from a linear combination of the signals from DQ and TQ filters also nulls these three phase coherences with less sensitivity to nonideal flip angles and with minor loss of sensitivity.

As in the one-pulse case, the five phase coherences obtained after the above two-pulse sequences are also characterized by an amplitude that is determined by relaxation rates and phase angles that accumulate over certain time intervals: (a) Phase coherence PC1 accumulates no phase. It is due entirely to the central transition. Its amplitude is determined by s_2 relaxation at all times. (b) Phase coherence PC2 starts to accumulate phase right after the first pulse and this accumulation is uninterrupted by the second pulse. (c) Phase coherence PC3 also starts to accumulate phase right after the first pulse, but the accumulation is stopped by the second pulse. (d) Phase coherence PC4 accumulates no phase in the first time interval τ, but, after the second pulse, it begins to accumulate phase as given by $\omega_Q(t - \tau)$. (e) Phase coherence PC5 is a spin echo. It accumulates a phase angle $\omega_Q\tau$ in the time interval between the first pulse and the beginning of the second pulse. The second pulse reverses this value to change the phase accumulation to $-\omega_Q\tau$. With further increase in time, the phase angle evolves as $\omega_Q(t - 2\tau)$ so that it increases from the negative value $-\omega_Q\tau$ after the second pulse and is zero at time $t = 2\tau$. At this time, the value of PC5 is independent of the value of ω_Q.

DISTRIBUTIONS OF QUADRUPOLE SPLITTINGS, ω_Q

Sodium NMR signals from salt-free xanthan gum solutions (*11*) and from sodium iodide solutions of κ-carrageenan (*12*) show separate peaks for the central and satellite transitions (liquid crystal behavior). This observed splitting into three separate peaks reflects a high degree of ordering of the macromolecules into fairly uniform domains with the same orientation in $\mathbf{B}_0$. Therefore, there is only one apparent ω_Q value. The smaller linewidth reported for the central transition compared to the satellite transition might indicate that $s_1 > s_2$. Alternatively, this inequality might be caused by a relatively narrow distribution of residual *eq* values.

It is possible that s_1 and s_2 can be different for different domains. For simplicity, the simulations described later in this paper assume that all domains have the same s_1 and s_2 values. Nevertheless, the simulation program can accommodate different values.

A ''powder'' sample in which all domains have the same *eq* and η values has a distribution of ω_Q values given by Eq. [25]. Each of the phase coherences for such samples is the sum taken over the Pake powder pattern distribution of ω_Q values. The NMR signal then is a linear combination of the various net phase coherences obtained with the numerical coefficients given in Table 1. From this point in the paper, the term ''PC1, PC2, . . . '' will denote the sum of a given phase coherence taken over all initial ω_Q values.

We can also encounter poorly ordered samples, such as biological tissue and many biopolymer gels, that have domains with a distribution of *eq* and also of η values. Such a situation would cause a large deviation from the Pake powder pattern. As can be shown by simulations, the resultant ω_Q distribution in such samples can be approximately Gaussian. Also, a variety of random physical processes are described by a Gaussian distribution, including NMR lineshapes in many solids. The mathematics of Gaussian distributions in such cases are well known and give simple relationships that are useful in deriving the behavior of NMR signals in limiting cases. In the limiting case of rapid motion, these relationships also describe the behavior of NMR signals from other distributions. Because there is not a simple equation for the Pake powder pattern distribution, we first examine the behavior of Gaussian phase coherences and relate them to observable NMR signals.

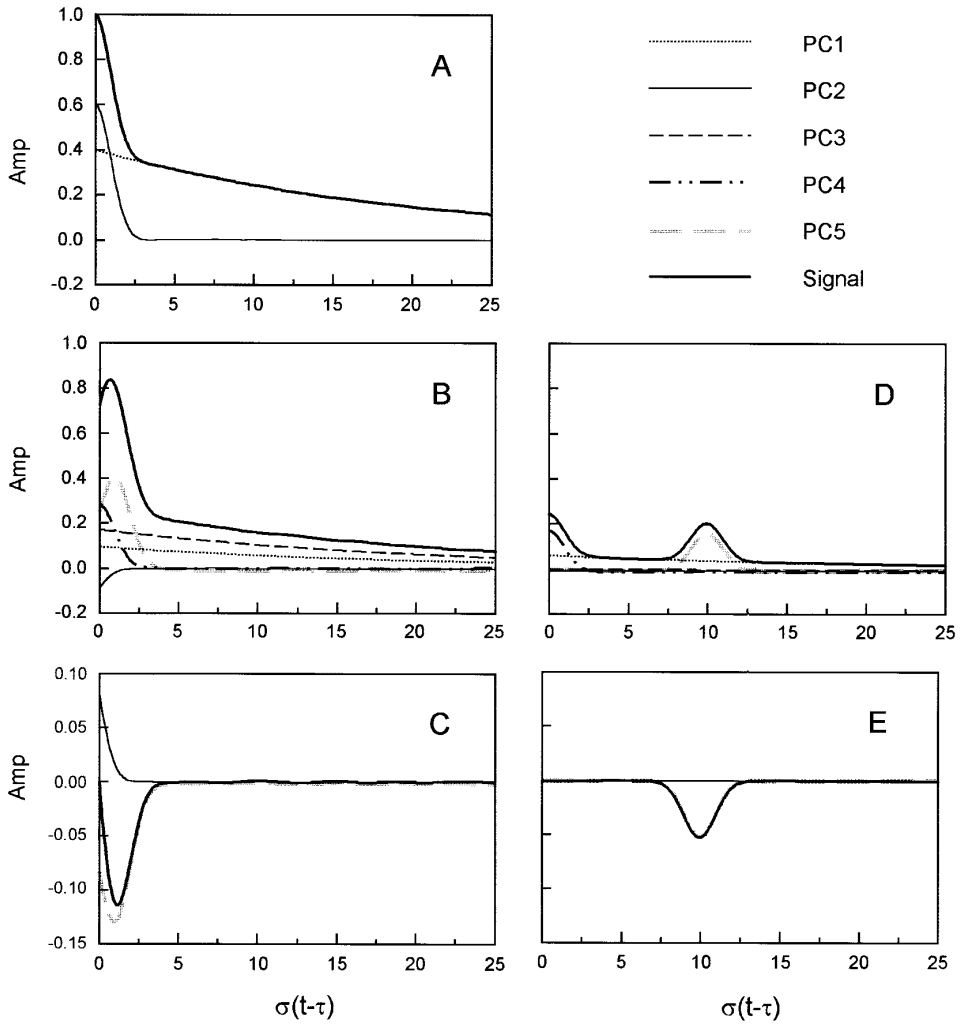

FIG. 1. Simulated phase coherences and NMR signals for the static case of a Gaussian distribution of ω_Q values with transverse relaxation rates $s_1 = s_2 = \sigma/20$. The horizontal axis in all cases is the time after the last pulse in the pulse sequence in units of $1/\sigma$. (A) The one-pulse signal. (B) The QE signal with $\tau = 1/\sigma$. (C) The DQ-MA signal with $\tau = 1/\sigma$. (D) The QE signal with $\tau = 10/\sigma$. (E) The DQ-MA signal with $\tau = 10/\sigma$.

NMR SIGNALS FROM GAUSSIAN DISTRIBUTIONS OF ω_Q VALUES

Gaussian Static Model

The one-pulse signal for the static Gaussian distribution of ω_Q is obtained by integrating Eq. [32] over the distribution of ω_Q values:

$$S(t) = (2/5)\exp(-s_2 t) + (3/5)\exp(-s_1 t)\exp(-\sigma^2 t^2/2)$$
$$= (2/5)\ \mathrm{PC1} + (3/5)\ \mathrm{PC2} \qquad [46]$$

This signal and the phase coherences PC1 and PC2 shown in Fig. 1A are calculated with the relaxation rates $s_1 = s_2 = \sigma/20$.

Phase coherence PC1 accumulates no phase. It is due entirely to the central transition. Its amplitude is determined by s_2 relaxation at all times.

Phase coherence PC2 decays rapidly after the pulse because the signals from different nuclei get out of phase with one another. After the time $t > 3/\sigma$, PC2 is small compared to the initial value and, even in highly ordered samples (Pake powder pattern distribution, see later discussion), it appears as minor wiggles ($\sim \pm 10\%$) of the NMR signal. Because the individual nuclei have phase memory, a subsequent refocusing pulse can produce a spin echo signal.

The QE signal for a static Gaussian distribution is

$$\mathrm{QE}(t > \tau) = (2/20)\exp(-s_2 t)$$
$$- (3/20)\exp[-s_1 t]\exp(-\sigma^2 t^2/2)$$
$$+ (6/20)\exp[-s_1 \tau]\exp[-s_2 (t-\tau)]\exp(-\sigma^2 \tau^2/2)$$
$$+ (6/20)\exp[-s_2 \tau]\exp[-s_1 (t-\tau)]$$

$$\times \exp[-\sigma^2(t-\tau)^2/2] + (9/20)\exp[-s_1 t]\exp[-\sigma^2(t-2\tau)^2/2] = 0.10\ \mathrm{PC1} - 0.15\ \mathrm{PC2} + 0.30\ \mathrm{PC3} + 0.30\ \mathrm{PC4} + 0.45\ \mathrm{PC5}. \quad [47]$$

Similarly, the DQ-MA signal is

$$\mathrm{MA}(t > \tau) = 0.141 \exp[-s_1 t]\exp(-\sigma^2 t^2/2) - 0.141 \exp[-s_1 t]\exp[-\sigma^2(t-2\tau)^2/2] = 0.141\ \mathrm{PC2} - 0.141\ \mathrm{PC5}. \quad [48]$$

The time behavior of these signals is, of course, determined by the behavior of the phase coherences and the value of τ. Figures 1B and 1C show the QE and DQ-MA phase coherences and the signals calculated for $\tau = 1/\sigma$. To illustrate the signals for longer τ values, Figs. 1D and 1E show these signals for $\tau = 10/\sigma$. As we show hereinafter, the phase coherences from the Pake powder pattern distribution are more complex.

Phase coherence PC2 starts to accumulate phase right after the first pulse and this accumulation is uninterrupted by the second pulse. Consequently, the net contribution from the nuclei of various ω_Q values after the second pulse is very small unless $\tau < 3/\sigma$ (compare Figs. 1D and 1E with 1B and 1C, respectively). It is due entirely to the satellite transitions and the relaxation is due to s_1 at all times.

Phase coherence PC3 also starts to accumulate phase right after the first pulse, but the accumulation is stopped by the second pulse. Consequently, the net contribution from the nuclei of various ω_Q values after the second pulse is also very small unless $\tau < 3/\sigma$, but it can be greater than for PC2 because the second pulse stops the phase accumulation.

Phase accumulation of PC4 commences right after the second pulse, as given by the product $\omega_Q(t - \tau)$. All the phase angles are zero right after this pulse. Because of the distribution of ω_Q values in a sample, the contributions from the various nuclei get out of phase and the net amplitude of this coherence decreases with time. It behaves like PC2 after the first pulse.

The second pulse acts to refocus part of the PC2 phase coherence from the first pulse and, because of the distribution of ω_Q values, phase coherence PC5 forms a spin echo at time $t = 2\tau$. The amplitude of this echo does not depend on the value of ω_Q in this static case. However, as shown in the following sections of this paper, any time dependence of ω_Q decreases the echo amplitude. This decrease augments the decrease caused by s_1 relaxation. Because the echo peak is far after the end of the pulse sequence, the echo amplitude is especially sensitive to any time dependence of ω_Q.

Each time domain NMR signal is a different linear combination of the phase coherences. Therefore, the various NMR signals are sensitive in different ways to the ω_Q distribution. This sensitivity allows us to use simulations to analyze various measured NMR signals and extract considerable information concerning size of the domains and the arrangement of macromolecules in the domains. We emphasize the time domain NMR signals because they can be less ambiguous than frequency domain spectra.

Gaussian Diffusion Model

When the domains are not extremely large, the translational diffusion of nuclei between domains with different ω_Q values causes ω_Q for a given nucleus to be time dependent, with consequent effects on the phase coherences. As indicated earlier, it is convenient to adopt the Gaussian frequency distribution model (*7*) in discussing general features of the effects of a time dependent ω_Q. In this model, ω_Q obeys a stationary random Gaussian distribution. The time dependence of ω_Q is embodied in the covariance function

$$\langle \omega_Q(t)\omega_Q(t+\tau)\rangle = \sigma^2 \exp(-\tau/\tau_e), \quad [49]$$

in which τ_e is the correlation time for the time dependence of ω_Q. The mathematics that leads to this relationship implies that the domains are arranged such that the successive ω_Q values experienced by a nucleus differ by only a small amount, as described by a small-step random diffusion process.

For the one-pulse case, the application of this model to Eq. [32] gives the following signal in the ''real'' channel of the receiver:

$$S(t) = (2/5)\exp(-s_2 t) + (3/5)\exp(-s_1 t) F_2(t). \quad [50]$$

Here,

$$F_2(t) = \exp\{-\sigma^2\tau_e^2[\exp(-t/\tau_e) - 1 + t/\tau_e]\} \quad [51]$$

replaces the cosine term in Eq. [32]. When τ_e is extremely long, $F_2(t)$ is nearly independent of the value of τ_e and reduces to the Gaussian decay function of the static case:

$$F_2(t) = \exp(-\sigma^2 t^2/2). \quad [52]$$

However, in the motionally narrowed limit when $\sigma^2\tau_e^2 \ll 1$, the functional form of $F_2(t)$ is the exponential decay function

$$F_2(t) = \exp(-\sigma^2 t\tau_e) \quad [53]$$

and the transverse magnetization after a single pulse is the sum of two exponential decays,

$$S(t) = (2/5)\exp(-s_2 t) + (3/5)\exp(-s_1' t) \quad [54]$$

where

$$s_1' = s_1 + \sigma^2 \tau_e. \quad [55]$$

This result shows that residual quadrupole splitting can give a biexponential relaxation decay in the motionally narrowed limit even when $s_1 = s_2$. Consequently, in this case it is inappropriate to use the observed biexponential rates to obtain a single correlation time to explain transverse relaxation. Unrecognized quadrupole splitting can be the dominant factor in causing observed biexponential transverse relaxation.

The same behavior occurs for the QE signal following two 90° pulses and the MQF signals. With proper definition of t, the cosine terms in PC2, PC3, and PC4 of Eq. [45] can be described by Eq. [51]. The final phase coherence, PC5, behaves differently, because the second pulse reverses the phase accumulated up to time τ. The cosine term in PC5 is replaced by the expression (*7, 19*)

$$F_5(t > \tau) = \exp\{-\sigma^2 \tau_e^2 [t/\tau_e - 3 - \exp(-t/\tau_e) + 2\exp(-\tau/\tau_e) + 2\exp\{-(t-\tau)/\tau_e\}]\}. \quad [56]$$

Note that when τ is very small, Eq. [56] reduces to Eq. [52] (which is the one-pulse case) and Eq. [33] reduces to Eq. [32]. When the conditions $\sigma\tau \gg 1$ and $\sigma\tau_e \gg 1$ are met simultaneously, a distinct spin echo (PC5) centered at time $t = 2\tau$ is formed. Also, when $\sigma^2\tau_e^2 \ll 1$, the functional form of $F_5(t > \tau)$ is the exponential decay function

$$F_5(t) = \exp(-\sigma^2 t \tau_e), \quad [57]$$

the same as Eq. [53].

Gaussian Distribution Random Jump Model

As mentioned earlier, samples can be poorly ordered so that the overall ω_Q distribution is nearly Gaussian. However, when the domains are arranged so that successive ω_Q values experienced by a nucleus can differ by large amounts, the Gaussian diffusion model is inappropriate and a Gaussian random jump model might be a better description of the time dependence of ω_Q.

The basic task in using Eqs. [32] and [45] to describe transverse magnetization when the ω_Q value of a given nucleus is time dependent is to evaluate averages of phase accumulation terms that have the form $\cos[\Phi(t)]$, where

$$\Phi(t) = \int_0^t \omega_Q(t)dt, \quad [58]$$

in which the distribution of $\omega_Q(t)$ values is stationary. The personal computer program CORVUS (Computations on Randomly Vitalized Uplifted Spins) is a simulator of the phase coherences when the ω_Q value of a nucleus undergoes random transitions among the values of a stationary distribution. CORVUS is adaptable to different models of incompletely disordered systems.

To evaluate $\Phi(t)$, we assume that a spin experiences a constant ω_Q for periods of various durations DUR. The value of DUR is chosen randomly (*20*):

$$\mathrm{DUR} = -\tau_e \log_e(\mathrm{RND}), \quad [59]$$

where RND is a new random number between 0 and 1. At the initial time, a value of ω_Q is chosen randomly from the distribution. At the end of the period DUR, a new value of ω_Q and the next value of DUR are chosen randomly. The value of Φ for a given nucleus after n durations is given by

$$\Phi_n = \sum_{i=1}^{n} \omega_{Qi} \mathrm{DUR}_i. \quad [60]$$

For the spin echo, the value of Φ accumulated from time $t = 0$ to $t = \tau$ is multiplied by -1 and further phase accumulation obeys Eq. [60]. To simulate a motionless system, a duration greater than the longest time in the computer experiment can be added to Eq. [59].

In the Gaussian distribution random jump model, CORVUS generates the ω_Q value as follows:

$$\omega_Q = \sigma\, \mathrm{GRND}, \quad [61]$$

where GRND is a Gaussian random number generated (*21*) by

$$\mathrm{GRND} = \{\sum_{i=1}^{12} \mathrm{RND}_i\} - 6, \quad [62]$$

in which each RND_i is a new random number between 0 and 1 and the rms value of GRND is 1.

NMR SIGNALS FROM POWDER PATTERN DISTRIBUTIONS OF ω_Q

Powder Pattern Random Jump Models

In contrast to the Gaussian models, the calculations in the CORVUS powder pattern models are based on domains that are tagged by orientation in $\mathbf{B}_0$. We assume a powder pattern distribution of θ and ϕ values. The values of ω_Q are generated by inserting θ and ϕ values into Eq. [25]. Let RND denote a random number between 0 and 1. Note the average value $\langle \mathrm{RND}^2 \rangle = 1/3$. Also, for a powder pattern we have the average value $\langle \cos^2\theta \rangle = 1/3$. Therefore, CORVUS chooses an initial orientation θ with a random number generator,

$$\cos\theta = \mathrm{RND} \quad [63]$$

$$\sin^2\theta = 1 - \mathrm{RND}^2, \quad [64]$$

and chooses the initial ϕ by generating a new random number and defining

$$\phi = 2\pi\,\mathrm{RND}. \quad [65]$$

After a residence time duration given by Eq. [59] with a new random number, a new orientation is chosen with the preceding equations.

Using this scheme, we can simulate the phase coherences for domains with chosen values of QCC and η. We can also perform simulations for less-than-perfect uniformity of domains. For example, we can let QCC values vary randomly between lower and upper limits and we can allow η to vary randomly between 0 and 1. Alternatively, we can choose a value of η and let the consecutive QCC values vary randomly over a Gaussian distribution that is centered on the average QCC value. We can easily generate other distributions with random numbers.

Many different ''random'' distributions of numbers VRND can be generated to define QCC distributions by generalizing Eq. [62]:

$$\mathrm{VRND} = \{\sum_{i=1}^{V} \mathrm{RND}_i\} - (V/2). \quad [66]$$

When $V = 1$, we obtain a square distribution. A triangular distribution is obtained with $V = 2$. For larger values of V we obtain bell-shaped distributions with different shapes. These shapes can be characterized by the ratio of the fourth moment to the second moment of the distribution of VRND. For $V = 12$ (''Gaussian'') this ratio is 2.92, which is very close to the theoretical value, exactly 3. This small difference is expected, because a true Gaussian distribution extends to infinity, whereas these distributions are truncated.

Powder Pattern Diffusion Model

The CORVUS powder pattern random jump models described earlier are different from diffusion models because they allow large changes in consecutive ω_Q values. In the limit $\sigma^2\tau_e^2 \ll 1$, all of these models give similar results. The case of infinitesimal consecutive changes in orientation with a single value of QCC and $\eta = 0$ (i.e., rotational diffusion) has been treated previously (*6*). However, when this limit is not met, the diffusion and jump models predict different dependences of the transverse magnetization on the value of τ_e (*3, 4*). The mathematical relationship between the amplitude of PC5 and the value of τ_e depends critically on the size of the reorientational jump. The time behaviors of the other phase coherences are much less sensitive to jump size.

CORVUS includes a powder pattern model that enables us to investigate the effects of various jump sizes. The initial orientation is generated randomly by Eqs. [63]–[65]. Subsequent orientations are then generated by angular rotations (instantaneous jumps) through the designated angle θ_J about an axis whose orientation is also chosen randomly by these equations (*20*). Reorientation by small jump angles approximates rotational diffusion. When this angle is small, the definition

$$\tau_J = \theta_J^2\tau_e, \quad [67]$$

where τ_J is the random jump time for this small angle (generated by a redefinition of Eq. [59]), relates this model to the Gaussian diffusion τ_e value. When $\tau > 5/\sigma$ and τ_e is large, the amplitude of PC5 at time $t = 2\tau$ depends exponentially on the third power of τ,

$$\mathrm{PC5}(2\tau) = \alpha\,\exp(-2s_1\tau)\exp[-a\tau^3], \quad [68]$$

for both Gaussian and powder pattern diffusion. This diffusion dependency is analogous to the echo attenuation caused by translational diffusion in a magnetic field gradient.

The corresponding dependency for both the Gaussian and the powder pattern random jump models is much different from that of the diffusion models:

$$\mathrm{PC5}(2\tau) = \beta\,\exp(-2s_1\tau)\exp[-b\tau]. \quad [69]$$

In Eqs. [68] and [69], a, b, α, and β are constants and may be different for the different models. With increasing ''diffusion'' jump angles, there is a transition of the dependency of PC5 on τ from Eq. [68] to Eq. [69].

SIMULATED NMR SIGNALS

Time Behavior of Phase Coherences

To simulate NMR signals for various models of motion and quadrupole frequency distributions, it is efficient to compute the individual phase coherences and then use the numerical coefficients given in Table 1 to calculate signals from specific RF pulse sequences. The simplest frequency distribution is Gaussian; the most complex distribution is the powder pattern with asymmetry parameter $\eta = 0$. These distributions are very different from each other; therefore, simulations with both are shown in this paper. Because the qualitative dependences of the signals on τ_e are similar for the diffusion and jump models, simulations only from the random jump models are shown. In discussing the general effects of quadrupole splitting on NMR signals, it is convenient to scale the time values in pulse sequences to $1/\sigma$. Figure 2 shows the phase coherences simulated with the Gaussian and powder pattern distributions for

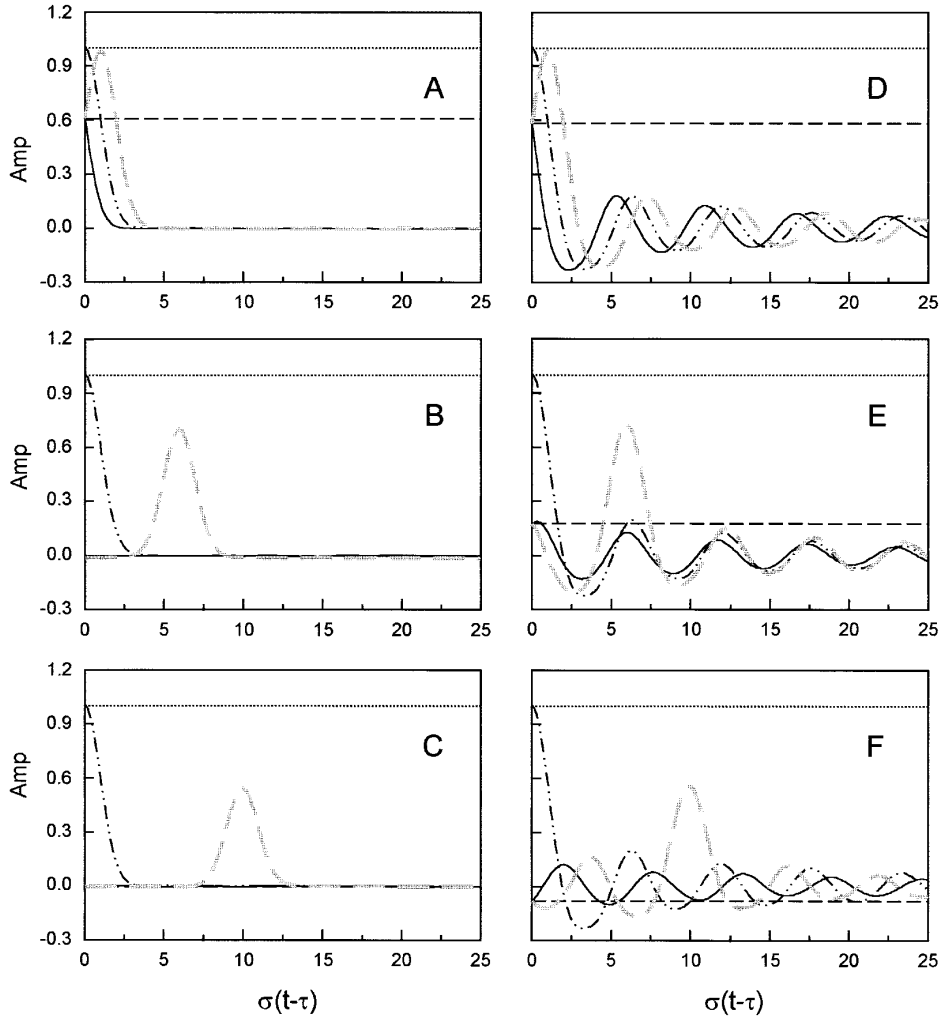

FIG. 2. Simulated phase coherences for the dynamic random jump cases of the Gaussian and powder pattern distributions of ω_Q values with transverse relaxation rates $s_1 = s_2 = 0$ and exchange time $\tau_e = 30/\sigma$. (A) Gaussian distribution with $\tau = 1/\sigma$. (B) Gaussian distribution with $\tau = 6/\sigma$. (C) Gaussian distribution with $\tau = 10/\sigma$. (D) Powder pattern distribution with $\eta = 0$ and $\tau = 1/\sigma$. (E) Powder pattern distribution with $\eta = 0$ and $\tau = 6/\sigma$. (F) Powder pattern distribution with $\eta = 0$ and $\tau = 10/\sigma$. The horizontal time axis is the same as in Fig. 1. The phase coherences are coded the same as in Fig. 1.

values of $\tau = 1/\sigma$, $6/\sigma$, and $10/\sigma$ with $\tau_e = 30/\sigma$. To emphasize the effects of residual quadrupole splitting, we set $s_1 = s_2 = 0$ in all cases. It is evident that the shapes of the coherences depend strongly on the distribution of ω_Q values. The powder pattern frequency distribution gives phase coherences that contain prominent wiggles when $\sigma\tau_e$ is large. The Gaussian distribution gives coherences that do not contain these wiggles. When feasible, NMR powder pattern signals simulated by CORVUS were validated by comparison with signals simulated by use of the general NMR simulation program ANTIOPE (*22*) provided by J. S. Waugh.

One-Pulse NMR Signals

Figure 3 shows the computed NMR signals for the random jump powder pattern frequency distribution for $\eta = 0$ and for the Gaussian random jump model plotted versus time for a range of $\sigma\tau_e$ values. To emphasize the effects of quadrupole splitting on the signals, the relaxation decay rates s_1 and s_2 are both chosen to be the same value, $\sigma/20$. Again, we scale the time values in these simulations to $1/\sigma$. In the powder pattern distribution, as we decrease τ_e the wiggles decrease in amplitude. When τ_e approaches $1/\sigma$, the period of the wiggles increases, representing exchange narrowing of the spectrum. When $\sigma^2\tau_e^2 \ll 1$, the initial portion of the curve is an exponential decay, obeying Eqs. [54] and [55]. The signals for the Gaussian random jump model, in contrast with the powder pattern signals, change little with decreasing τ_e until τ_e approaches $1/\sigma$ because the wiggles do not occur. With further decreasing τ_e values, the curves for these two models become increasingly similar and are virtually identical when $\sigma\tau_e = 0.1$.

For both of these models, the initial portions of these curves are Gaussian and virtually indistinguishable when $\sigma\tau_e$ is not

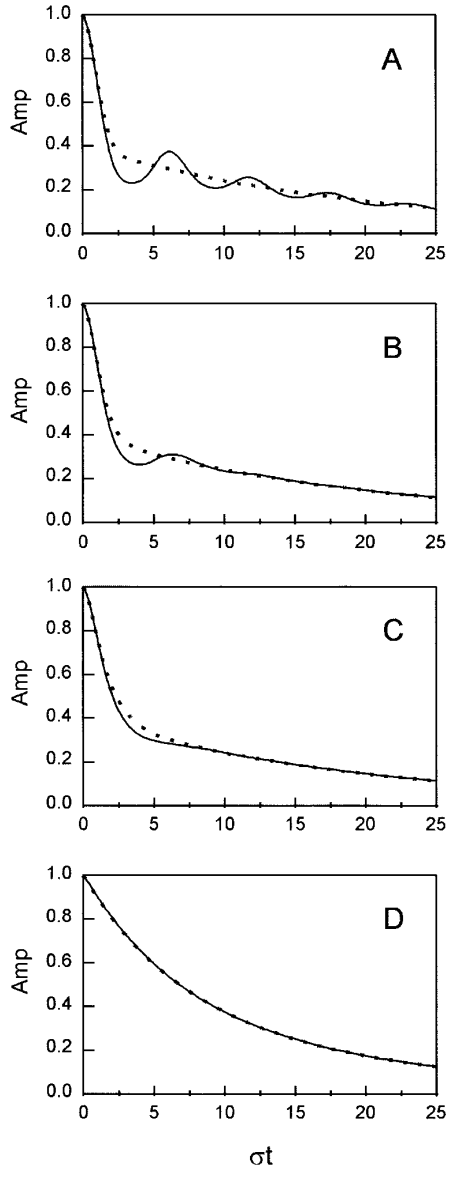

FIG. 3. Simulated one-pulse NMR signals for the powder pattern distribution with $\eta = 0$ (solid line) and the Gaussian distribution with transverse relaxation rates $s_1 = s_2 = \sigma/20$. (A) $\tau_e = 30/\sigma$. (B) $\tau_e = 3/\sigma$. (C) $\tau_e = 1/\sigma$. (D) $\tau_e = 0.1/\sigma$. The horizontal time axis is the same as in Fig. 1.

small. This is characteristic of transverse magnetization in samples with nonrandom ordering (*23–27*). Because of this initial Gaussian character, conventional interpretation of T_2 measurements in terms of exponential functions can overestimate the number of nuclei with the shorter T_2 value. This can cause deviations from the 60/40 ratio of short versus long T_2 components. Errors in quantitation of the number of spin 3/2 nuclei in the sample can also result.

Quadrupole Echo and Multiple-Quantum-Filter NMR Signals

Phase coherences PC2, PC3, and PC4 include phase accumulation that starts at particular times in the pulse sequence and are related to the signal following one pulse, with appropriate choice of specific time interval. The preceding simulations indicate that there is no clear, direct indication of residual quadrupole splitting in the one-pulse signals from very disordered samples (i.e., absence of wiggles such as occurs with a Gaussian distribution). However, phase coherence PC5 forms a spin echo at time $t = 2\tau$ that is caused by the quadrupole splitting and is most prominent in the quadrupole echo and DQ-MA signals. Figure 4 shows the quadrupole echo and DQ-MA signals at $\tau = 1/\sigma$, $6/\sigma$, and $10/\sigma$ for the powder pattern random jump model and Gaussian distribution random jump model for $\tau_e = 50/\sigma$ and $s_1 = s_2 = \sigma/20$. The Gaussian signals in Fig. 4 show that, even in a disordered sample with exchange between domains, PC5 provides a prominent spin echo that results from residual quadrupole splitting. Figure 5 shows the quadrupole echo and DQ-MA signals at $\tau = 6/\sigma$ and $10/\sigma$ from the Gaussian distribution random jump model for exchange that is faster than used in Fig. 4, $\tau_e = 10/\sigma$. Comparison of Figs. 4 and 5 shows that the spin echo amplitude (PC5) is especially sensitive to the exchange time τ_e and decreases with decreasing values of τ_e.

DISCUSSION

Transverse Relaxation in the Motionally Narrowed Limit

The NMR signal characteristics in the motionally narrowed limit for the Gaussian distribution of ω_Q values also apply to signals from the other frequency distributions and ω_Q time dependences presented in this paper. The successive values of ω_Q for a given nucleus in the Pake powder pattern frequency distribution are determined by the orientations. When the condition $\sigma^2\tau_e^2 \ll 1$ is met, the phase angle accumulated during residence in a given value of ω_Q is much less than 1 radian (i.e., $\sigma\tau_e \ll 1$). This limit is met when the domains are sufficiently small so that τ_e is also small. Because this is also the condition for validity of a small-step diffusion model, all these models agree with the Gaussian frequency distribution diffusion model, and it provides a convenient mathematical framework for presenting the results of the various models in this limit. In this limit of motion, s_1 in all the NMR signals treated here is effectively replaced by $s_1' = s_1 + \sigma^2\tau_e$. This holds for all of the ω_Q distributions and time dependences described in this paper. Therefore, short-range residual quadrupole splitting can cause biexponential transverse relaxation behavior in all these NMR signals even when $s_1 = s_2$. When $s_1 \approx s_2$ and τ_e is sufficiently short so that $\sigma^2\tau_e \leq s_1$, the transverse relaxation can appear to be monoexponential.

The central focus of this paper is on the effects of the strength and of the time dependence of the residual quadrupole interaction on the NMR signals following several different RF pulse sequences. These effects are parts of the exchange/motional narrowing problem (*7*). Of course, the τ_e values can contribute to the distribution of correlation times described by Springer (*28, 29*). In

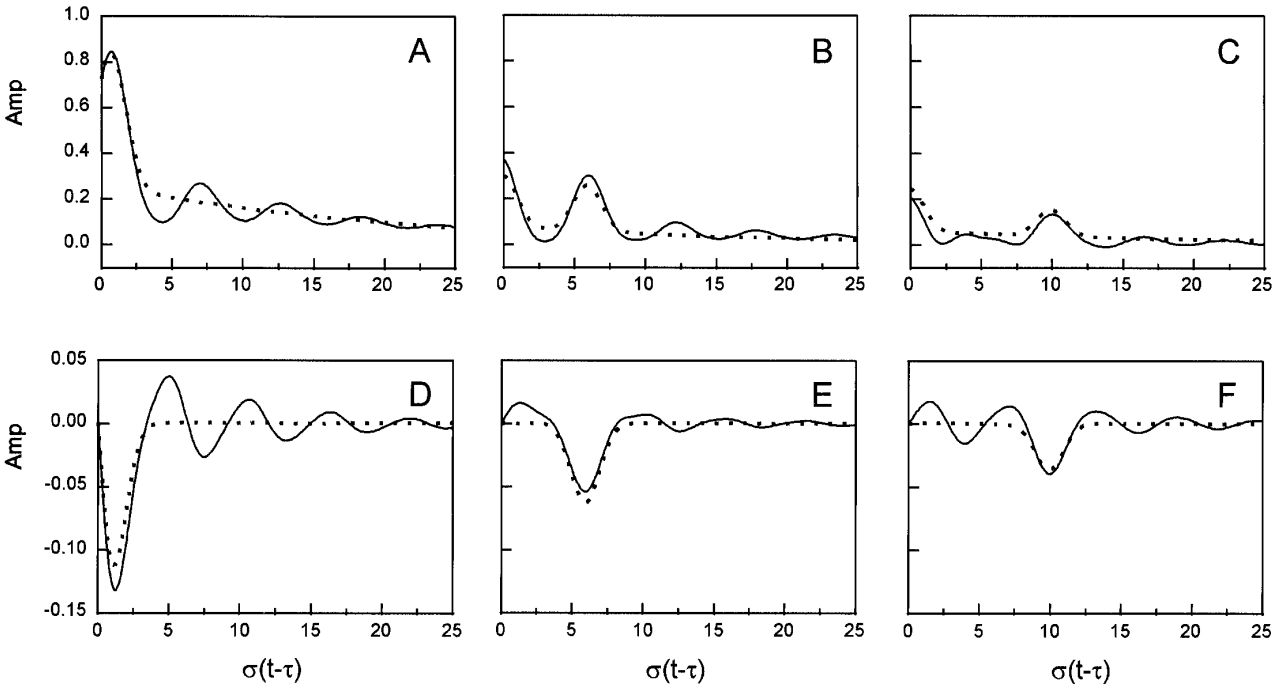

FIG. 4. Simulated QE (A, B, and C) and DQ-MA (D, E, and F) NMR signals for the powder pattern distribution with $\eta = 0$ (solid line) and the Gaussian distribution with transverse relaxation rates $s_1 = s_2 = \sigma/20$ and exchange time $\sigma\tau_e = 50/\sigma$. (A and D) $\tau = 1/\sigma$. (B and E) $\tau = 6/\sigma$. (C and F) $\tau = 10/\sigma$. The horizontal time axis is the same as in Fig. 1.

the domain model, we assume that τ_e is large compared to $1/\omega_0$. The residual quadrupole interaction is relatively ineffective in causing the energy level transitions that dominate in the spectral densities $J_1(\omega_0)$ and $J_2(2\omega_0)$ because (a) it is small compared to the ^{23}Na nuclear quadrupole interaction with the electric dipole moment of a water molecule or with an electric charge and (b) the spectral density is proportional to the square of the interaction. However, it can be the dominant factor in determining $J_0(0)$ or the shape of the NMR signal.

Many of the characteristics of ^{23}Na NMR signals in aqueous heterogeneous samples can be described within the conceptual framework of domains with different residual ω_Q values and with migration or exchange of Na^+ ions between these domains. The observations of quadrupole splitting of ^{23}Na in ''powder samples'' of xanthan gum solutions (*11*) and κ-carrageenan solutions (*12*) indicate large values of τ_e such that $\sigma\tau_e \gg 1$. Also, biexponential transverse relaxation of ^{23}Na in agarose gels (*30*) without apparent quadrupole splitting agrees with the condition $\sigma^2\tau_e^2 \ll 1$ so that s_1 is effectively replaced by $s_1' = s_1 + \sigma^2\tau_e$. If the condition $s_1 \approx s_2$ is met, the biexponential relaxation character means that τ_e is sufficiently long to cause $\sigma^2\tau_e \gg s_2$. If we continue in this progression, we see that the reported monoexponential transverse relaxation in gelatin gels (*1*, *30*) agrees with effectively smaller domains, compared to agarose gels, such that $\sigma^2\tau_e \leq s_2$. Generalizing this concept of domains, it is possible to have hierarchies of domains such that clusters of small nonrandomly oriented domains are themselves ordered into larger domains. In this way, a variety of different orderings of macromolecules can be included in the domain concept.

Detection of Residual Quadrupole Splitting

The quadrupole echo RF pulse sequence is the most direct, simplest detector of residual quadrupole splitting and exchange of sodium ions between different domains, especially when $\sigma\tau_e$ is large. Many samples might have domains that have a range of QCC and η values, making observation of residual quadrupole splitting from wiggles on the one-pulse NMR signal difficult or impossible. In the absence of exchange, the refocusing action of the second pulse produces the spin echo at time $t = 2\tau$ from PC5. The spin echo amplitude is independent of the exact QCC and η values and provides a ready means of detecting residual quadrupole splitting. With the onset of exchange, the sensitivity of the spin echo amplitude to $\sigma\tau$ and $\sigma\tau_e$ allows us to determine $\sigma\tau_e$. However, if the sample is compartmentalized so that only a fraction of the nuclei have $\sigma \neq 0$, the DQ and, especially, the DQ-MA signals might be preferable for analyzing many complex systems. This is because the DQ-MA signal contains only the contributions from the satellite transitions.

The initial value of MQF signals, right after the pulse sequence, is zero. Because of this important property, the MQF signal is zero at all later times unless some of the phase coherences have different dependences on time. To observe a nonzero MQF signal for times $t > \tau$, the *minimum* requirement is *either* that $\sigma \neq 0$ or $s_1 \neq s_2$.

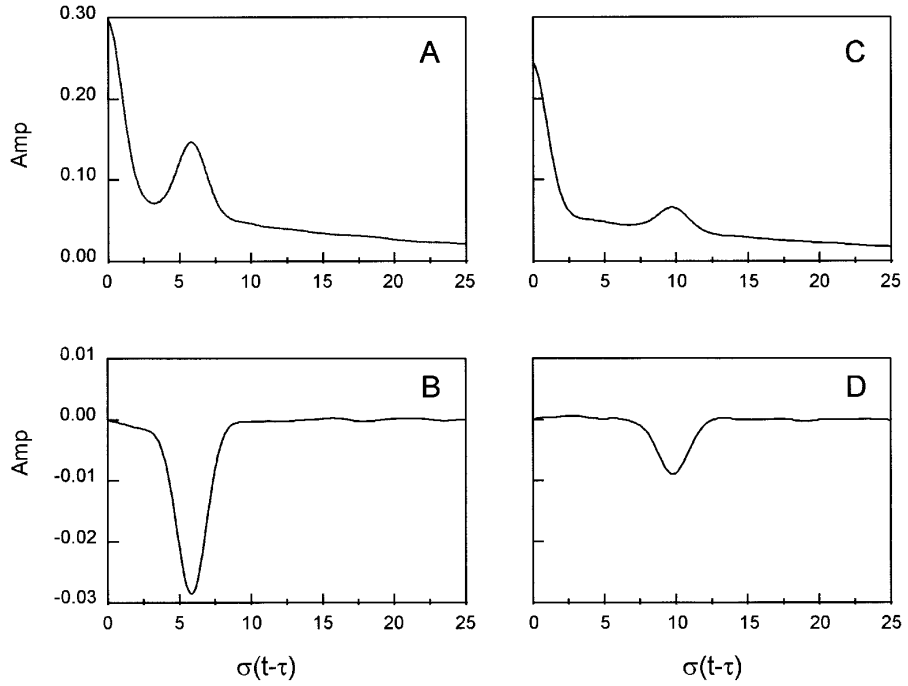

FIG. 5. Simulated QE (A and C) and DQ-MA (B and D) NMR signals for the Gaussian distribution with transverse relaxation rates $s_1 = s_2 = \sigma/20$ and exchange time $\tau_e = 10/\sigma$. (A and B) $\tau = 6/\sigma$. (C and D) $\tau = 10/\sigma$. The horizontal time axis is the same as in Fig. 1.

When $\sigma = 0$, that is, when there is no *residual* local efg, there is no echo signal and both the DQ and TQ filters give signals that obey the equation

$$S(t > \tau) = C_n\{\exp[-s_2\tau] - \exp[-s_1\tau]\} \times \{\exp[-s_2(t-\tau)] - \exp[-s_1(t-\tau)]\}, \qquad [70]$$

where the numerical coefficient C_n for the DQ filter is 0.106 and for the TQ filter is 0.159. The condition $s_1 \neq s_2$ allows a nonzero MQF signal. On the other hand, the DQ-MA filter and the composite 3DQ–2TQ filter both depend on relaxation rate s_1 only and their MQF signal is zero when there is no residual local efg. This feature makes these filters specific for the detection of residual quadrupole splitting.

When $\sigma \neq 0$, all of the MQFs can give nonzero signals even when $s_1 = s_2$. In the case of rapid exchange ($\sigma^2\tau_e^2 \ll 1$), the MQFs can give signals that are approximated by Eq. [70] because s_1 is replaced by $s_1' = s_1 + \sigma^2\tau_e$. When $\sigma\tau_e$ is larger in value, the various filters give signals with different time dependences after the pulse sequence. The TQ filter signal has the same algebraic sign at all times and the residual quadrupole splitting shows up in the shape of the time-dependent signal. This shape depends on the order in the sample and on the values of $\sigma\tau$ and $\sigma\tau_e$. Even though the TQ filter gives the greatest signal amplitude, its utility in discriminating quadrupole splitting when $s_1 \neq s_2$ is the weakest among the multiple quantum filters.

The effects of ordering and structure in the domains are embodied in the values of σ and τ_e. The DQ filter gives negative signals when $\tau \leq 5/\sigma$. Because the negative excursion is the greatest when $\tau \approx 1/\sigma$, the measurement of the DQ signal as a function of τ allows an estimate of the value of σ even when the ordering in the sample is poor.

The DQ-MA filter is more incisive in this estimation, because it includes only the phase coherences PC2 and PC5. These coherences depend only on s_1 relaxation and on residual quadrupole splitting, but have maxima that occur in different time periods. When $\sigma \neq 0$, and when we increase the preparation time τ starting from zero, the DQ-MA filter time domain signal changes as follows. When τ is zero, the magnitude of this signal is zero. With somewhat larger values of τ, a signal appears with a ''peak'' that occurs at time $(t - \tau) \approx 1/\sigma$ after the pulse sequence. With increasing τ, the magnitude of the peak of this signal increases and passes through a maximum when $\tau \approx 1/\sigma$. Then, with further increases in τ, this peak in the time domain signal moves to greater times and eventually occurs at $t = 2\tau$. Simultaneously, the signal shape becomes more complex. Because of the absence of wiggles, the signals from the Gaussian distribution are the least complex. When a distinct echo signal occurs, the absence of wiggles may imply that a Gaussian distribution is a reasonable description of the ω_Q values for the sample.

As shown in Fig. 4D–F for the Gaussian distribution, increasing the preparation time to values greater than $\tau \approx 3/\sigma$ causes the DQ-MA signal to remain very small for increasingly greater time intervals. This time interval has significant con-

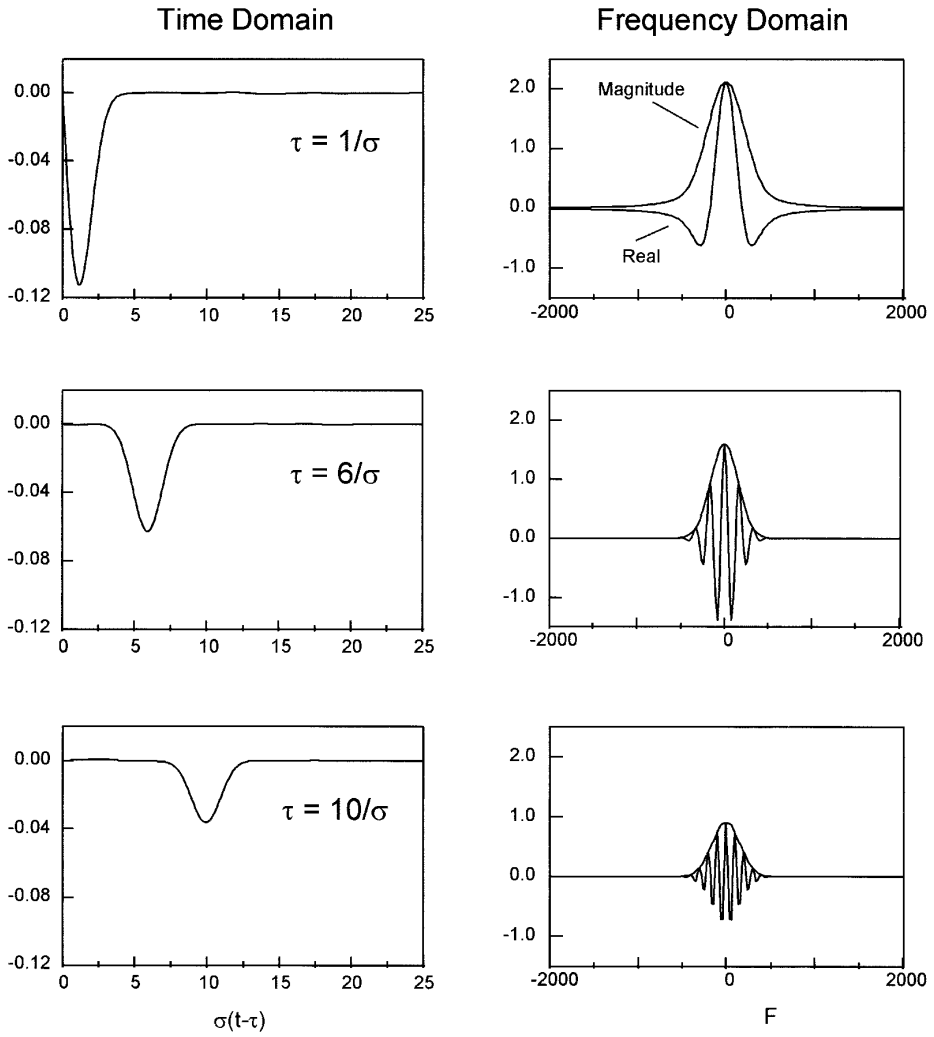

FIG. 6. Simulated time domain DQ-MA NMR signals of the Gaussian distribution in Fig. 4 and the frequency domain spectra of these signals. The horizontal time axis is the same as in Fig. 1.

sequences in the NMR spectrum that is the Fourier transform of this time domain signal. Figure 6 shows the Fourier transform of the Gaussian distribution DQ-MA signals of Fig. 4. For preparation times shorter than $\tau \approx 3/\sigma$, the Fourier transform gives a spectrum with a broad peak which is superposed on a narrower peak that is of opposite algebraic sign. For preparation times greater than $\tau \approx 3/\sigma$, the increasing time range of small signal values gives an increasingly complex spectrum. Wiggles appear and the number of them in the spectrum increase with increase in τ. These wiggles from the ''wiggle free'' Gaussian quadrupole frequency distribution result from the time shift of the signal maximum and do not represent structural parameters in the sample. It is clear that the shift of the time domain signal maximum to longer times gives spectra that are increasingly difficult to analyze and that the time domain signal gives more direct, less ambiguous information.

The preceding results suggest that simulations based on the five phase coherences can aid in interpreting and quantifying one-pulse, QE, and multiple-quantum-filter signals from spin 3/2 nuclei. This has been demonstrated (*14*) for ^{23}Na in a sample composed of 1.0 ml of 100 mM aqueous NaCl and 0.2 g xanthan gum. We have also observed ^{23}Na quadrupole splitting in other aqueous biopolymers such as welan gum and rhamsan gum. When interpreting such data it should be realized that, because s_1 and σ are both active in the same time intervals, a value of the spin echo amplitude that is less than the value of coefficient $c5$ in Table 1 can be a consequence either of s_1 relaxation or exchange between domains of different ω_Q values, or of a combination of both possibilities.

One last point worth mentioning is that agarose gels give a null DQ-MA signal and hence do not show direct evidence of quadrupole splitting such has been reported for biological tissue (*1*, *2*). Therefore, gels of a different biopolymer, such as xanthan gum, may be more appropriate phantoms for ^{23}Na in biological tissue.

CONCLUSIONS

Residual quadrupole splitting from anisotropic interactions between quadrupolar nuclei and local ordered arrangements of macromolecules can greatly affect the NMR signals following one-pulse, QE, and MQF pulse sequences. This splitting acts as a tag that sensitizes the nucleus to the macromolecular arrangements that it experiences as it diffuses in the sample. Failure to recognize the results of residual quadrupole splitting on NMR signals can lead to misinterpretation of NMR relaxation measurements. The signals from these pulse sequences can be simulated for many different structural and dynamical physical models. These simulations can be used to interpret NMR signals in terms of the physical parameters in these models, leading to increased understanding of structure and ion binding in samples such as biological tissue and biopolymer gels.

ACKNOWLEDGMENTS

The authors thank Dr. J. S. Waugh for his versatile NMR simulation program ANTIOPE and for invaluable discussions concerning the simulation of random events in NMR. This work was supported in part by Alcon Laboratories of Fort Worth, TX, the Whitaker Foundation, and the National Institutes of Health (Grants R29 HL54574 and RR02584). We also thank Professor A. Dean Sherry for his helpful comments during the preparation of this manuscript.

REFERENCES

1. U. Eliav and G. Navon, Analysis of double-quantum-filtered NMR spectra of ^{23}Na in biological tissues, *J. Magn. Reson. B* **103,** 19–29 (1994).
2. R. Reddy, L. Bolinger, M. Shinnar, E. Noyszewski, and J. S. Leigh, Detection of residual quadrupolar interaction in human skeletal muscle and brain *in vivo* via multiple quantum filtered sodium NMR spectra, *Magn. Reson. Med.* **33,** 134–139 (1995).
3. D. E. Woessner and B. S. Snowden, Jr., A pulsed NMR study of dynamics and ordering of water molecules in interfacial systems, *Ann. NY Acad. Sci.* **204,** 113–124 (1973).
4. D. E. Woessner, Nuclear magnetic relaxation and structure in aqueous heterogeneous systems, *Mol. Phys.* **34,** 899–920 (1977).
5. D. E. Woessner and B. S. Snowden, Jr., NMR doublet splitting in aqueous montmorillonite gels, *J. Chem. Phys.* **50,** 1516–1523 (1969).
6. D. E. Woessner, B. S. Snowden, Jr., and G. H. Meyer, Calculation of NMR free induction signals for nuclei of molecules in a highly viscous medium or a solid–liquid system, *J. Chem. Phys.* **51,** 2968–2976 (1969).
7. D. E. Woessner, Brownian motion and its effects in NMR chemical exchange and relaxation in liquids, *Concepts in Magnetic Resonance* **8,** 397–421 (1996).
8. H. J. C. Berendsen and H. T. Edzes, The observation and general interpretation of sodium magnetic resonance in biological material, *Ann. NY Acad. Sci.* **204,** 459–485 (1973).
9. B. Halle, H. Wennerström, and L. Piculell, Interpretation of counterion spin relaxation in polyelectrolyte solutions, *J. Phys. Chem.* **88,** 2482–2494 (1984).
10. C. S. Springer, Jr., Biological systems: Spin 3/2 nuclei, *in* ''The Encyclopedia of Nuclear Magnetic Resonance'' (D. M. Grant and R. K. Harris, Eds.), pp. 940–951, Wiley, New York (1996).
11. L. Bezemer and J. C. Leyte, Behavior of native xanthan in the biphasic region: a ^{23}Na counterion NMR study, *J. Phys. Chem.* **99,** 3743–3747 (1995).
12. J. Borgström, P.-O. Quist, and L. Piculell, A novel chiral nematic phase in aqueous κ-carrageenan, *Macromolecules* **29,** 5926–5933 (1996).
13. R. Reddy, S. Li, J. B. Kneeland, and J. S. Leigh, *In vivo* sodium multiple quantum spectroscopy of human articular cartilage, Proceedings of the International Society for Magnetic Resonance in Medicine, Fourth Scientific Meeting and Exhibition, Vol. 1, p. 32, 1996.
14. D. E. Woessner and N. Bansal, Effect of motion on quadrupole splitting of spin 3/2 nuclei, Proceedings of the International Society for Magnetic Resonance in Medicine, Fifth Scientific Meeting and Exhibition, Vol. 1, p. 247, 1997.
15. D. E. Woessner, unpublished calculations (1978).
16. G. Jaccard, S. Wimperis, and G. Bodenhausen, Multiple-quantum NMR spectroscopy of S = 3/2 spins in isotropic phase: A new probe for multiexponential relaxation, *J. Chem. Phys.* **85,** 6282–6293 (1986).
17. R. Reddy, M. Shinnar, Z. Wang, and J. S. Leigh, Multiple-quantum filters of spin-3/2 with pulses of arbitrary flip angle, *J. Magn. Reson. B* **104,** 148–152 (1994).
18. N. Müller, G. Bodenhausen, and R. R. Ernst, Relaxation induced violations of coherence transfer selection rules in nuclear magnetic resonance, *J. Magn. Reson.* **75,** 297–334 (1987).
19. J. R. Klauder and P. W. Anderson, Spectral diffusion decay in spin resonance experiments, *Phys. Rev.* **125,** 912–932 (1962).
20. J. S. Waugh, personal communication (1996).
21. J. H. Noggle, ''QuickBasic Programming for Scientists and Engineers,'' p. 128, CRC Press, Ann Arbor, MI (1993).
22. F. Stickney de Bouregas and J. S. Waugh, ANTIOPE, a program for computer experiments on spin dynamics, *J. Magn. Reson.* **96,** 280–289 (1992).
23. J. Charvolin and P. Rigny, Pulsed NMR in dynamically heterogeneous systems, *J. Magn. Reson.* **4,** 40–46 (1971).
24. J. Charvolin and P. Rigny, Proton relaxation study of paraffinic chain motions in a lyotropic liquid crystal, *J. Chem. Phys.* **58,** 3999–4008 (1973).
25. J. P. Cohen-Addad, Effect of the anisotropic chain motion in molten polymers: The solidlike contribution of the nonzero average dipolar coupling to NMR signals. Theoretical description, *J. Chem. Phys.* **60,** 2440–2453 (1974).
26. J. P. Cohen-Addad and R. Vogin, Molecular motion anisotropy as reflected by a ''pseudosolid'' nuclear spin echo: Observation of chain constraints in molten *cis*-1,4-polybutadiene, *Phys. Rev. Lett.* **33,** 940–943 (1974).
27. M. Bloom, E. E. Burnell, S. B. W. Roeder, and M. I. Valic, Nuclear magnetic resonance line shapes in lyotropic liquid crystals and related systems, *J. Chem. Phys.* **66,** 3012–3020 (1977).
28. W. D. Rooney and C. S. Springer, Jr., A comprehensive approach to the analysis and interpretation of the resonances of spins 3/2 from living systems, *NMR Biomed.* **4,** 209–226 (1991).
29. W. D. Rooney and C. S. Springer, Jr., The molecular environment of intracellular sodium: ^{23}Na NMR relaxation, *NMR Biomed.* **4,** 227–245 (1991).
30. G. S. Payne and P. Styles, Multiple-quantum-filtered ^{23}Na NMR spectroscopy in model systems, *J. Magn. Reson.* **95,** 253–266 (1991).